International Journal of Railway Research, Vol. 7, No. 2, (2020), 19-33

Iran University of Science and Technology

International Journal of

Railway Research

An Innovative Method for Sloshing Analysis of a Partially-Filled Tank Wagon in Braking Using a Coupled Vehicle/Fluid Model

Ahmad Rahmati-Alaei [1], Majid Sharavi[1*], Masoud Samadian Zakaria[2]

[1]School of Railway Engineering, Iran University of Science and Technology, Tehran, Iran

[2]School of Mechanical Engineering, K.N. Toosi University of Technology, Tehran, Iran

ARTICLE INFO

Article history:
Received: 8.06.2020
Accepted: 14.08.2020
Published: 25.12.2020

Keywords:
Tank wagon
Transient fluid slosh
Wagon dynamic
Coupled model
Braking

A B S T R A C T

In this paper, an innovative method as a coupled numerical model is developed for assessing the interaction between wagon dynamics and transient fluid slosh. This model can be considered as a robust and effective computational tool for investigation of sloshing in tank vehicles in different tank conditions and maneuvers. Fourth-order Runge-Kutta method is adopted for solving the 19 degrees of freedom (DOFs) wagon dynamics model. The three-dimensional model is adopted, which includes car body, bogies and wheel-axles with longitudinal, vertical, pitch, and roll vibrations. Transient fluid slosh is analyzed using the computational fluid dynamics method (CFD) based on the Navier–Stokes equations combined with the volume of fluid technique (VOF). Also, the sloshing test setup is developed for validation of the multi-phase CFD simulation. By coupling of the wagon dynamics model with the fluid slosh model, the dynamic response characteristics of the railway tanker are analyzed under straight-line braking maneuvers. The numerical parametric study is conducted to investigate the effect of filling volume and viscosity.

1. Introduction

Each year, a significant number of derailments are reported for freight wagons. [1] This issue becomes more important for partially filled railway tank wagon because of their instability in various maneuvers, such as braking and turning, is strongly influenced by the movement of fluid inside the tank. The basic problem in fluid slosh is the calculation of forces, moments, and also the natural frequencies of the fluid flow, which affects the dynamics of the vehicle.

Fundamentally these depend on parameters such as filling volume, fluid properties, tank geometry, baffles, and type of excitation. In recent studies, fluid slosh in partially-filled tank vehicles has been investigated in various methods, including quasi-static, mechanical analogy and more complex models such as the vehicle dynamics coupled with the computational fluid dynamics (CFD).

In the quasi-static method, the fluid is assumed to move in the form of a rigid body.[2, 3] Kang, Rakheja [4] combined a quasi-static model of a partially-filled tank with three-dimensional (3D) vehicle model under longitudinal and lateral acceleration. Their results show that in the braking maneuvers in the curved track, the vehicle is much more under rollover. This method only allows the stability analysis of the vehicle in steady-state condition and cannot be used to investigate the effects of transient slosh on situations such as baffles [5-7] Modaressi-Tehrani, Rakheja [8] showed that the forces and moments of transient fluid slosh are essentially larger than the steady-state values in quasi-static methods.

The mechanical analogy method is based on the linear slosh theory and assumptions

*Corresponding author, Assistant professor
Email: m_shahravi@iust.ac.ir

[DOI: 10.22068/IJRARE.7.2.19]

including inviscid fluid and irrotational flows. The fluid is modelled as a series of mass-spring-damper or simple pendulums, assuming linear fluid motion [9]. The stiffness of the springs and the length of the pendulum are obtained from the natural frequencies of fluid slosh. Since the equations of motion for lumped masses are usually included easily in the general motion equation of vehicles, this method has attracted a lot of attention in the field of automotive engineering. [9]

Salem, Mucino [10] simulated the lateral sloshing in a partially-volume elliptical tanker with equivalent trammel pendulums. Their model can be considered as a computationally effective tool for analyzing coupling between fluid slosh and vehicle dynamics in low amplitude excitations. Younesian, Abedi [11] combined the equivalent spring-damper model of fluid sloshing with a wagon dynamic system. They showed that ignoring the fluid slosh may cause 18% and 25%, error in the computing of derailment quotient and unloading ratio, respectively.

The mechanical analogy method has complexities in estimating the non-linear parameters affected by the large slosh wave excitation, particularly in complex tank geometries with baffles and simultaneous lateral and longitudinal maneuvers [9, 12, 13]. Rahmati and Shahravi [14] compared the accuracy of the equivalent mechanical model for a partially-filled tank with a three-dimensional explicit finite elemental model during a turning maneuvers. They showed that in low filling volumes (15% and less), the frequency and amplitude of fluid slosh for the two previous models differ by less than 5%. Therefore, in the low filling volumes, an equivalent mechanical model can be used because of the saving in time and cost of calculation.

An effective method for assessing the stability of partially-filled tanker is the coupled vehicle dynamics-CFD procedure. Coupled analysis has led to fewer studies due to its complexity. The calculations are made in two subsystems, including fluid slosh and vehicle dynamics, in which both the two models simultaneously exchange input and output data in predetermined time steps [5, 6, 15]. The CFD analysis allows the calculation of forces and moments of fluid slosh in a transient and a high amplitude excitation. D'ALESSANDRO [9] and Thomassy, Wendel [16] studied the braking and steering response of the partially-filled tank truck by combining CFD and vehicle dynamics models.

Azadi, Jafari [17] coupled the liquid sloshing model with the vehicle dynamics model, which is based on the Navier–Stokes equations combined with the volume of fluid (VOF) technique and then evaluated the effects of different tank geometry on the tractor semi-trailer vehicle dynamics. Although the effects of fluid slosh have been studied on the dynamic characteristics of road tankers in automotive engineering relatively few studies have been devoted to the coupling of CFD model with multibody system (MBS) in railway engineering by considering nonlinear wheel-rail contact [18]. The forces and moments resulting from the fluid slosh and its effect on the 3D wheel-rail contact make it a complex problem and will lead to a derailment.

In this paper, an innovative method is developed as a coupled numerical model. The differential equations of motion for a three-dimensional model of a wagon by 19-degrees of freedom (DOFs), including longitudinal, vertical, roll and pitch vibrations, are obtained using the energy method. The vibration response of the wagon dynamics model is obtained using the fourth-order Runge-Kutta method. The transient fluid slosh model has been solved using the CFD method based on the Navier–Stokes equations combined with VOF technique.

The CFD model is validated with experimental fluid slosh data. Then, the dynamic response of the railway tanker is obtained under the fluid slosh in the straight line braking with the coupling of the two previous models. The coupling procedure is such that the force and moment of fluid slosh are considered in the wagon dynamics model as the terms of forced vibration. A parametric study for the coupled model is done on the filling volume and fluid viscosity.

[DOI: 10.22068/IJRARE.7.2.19]

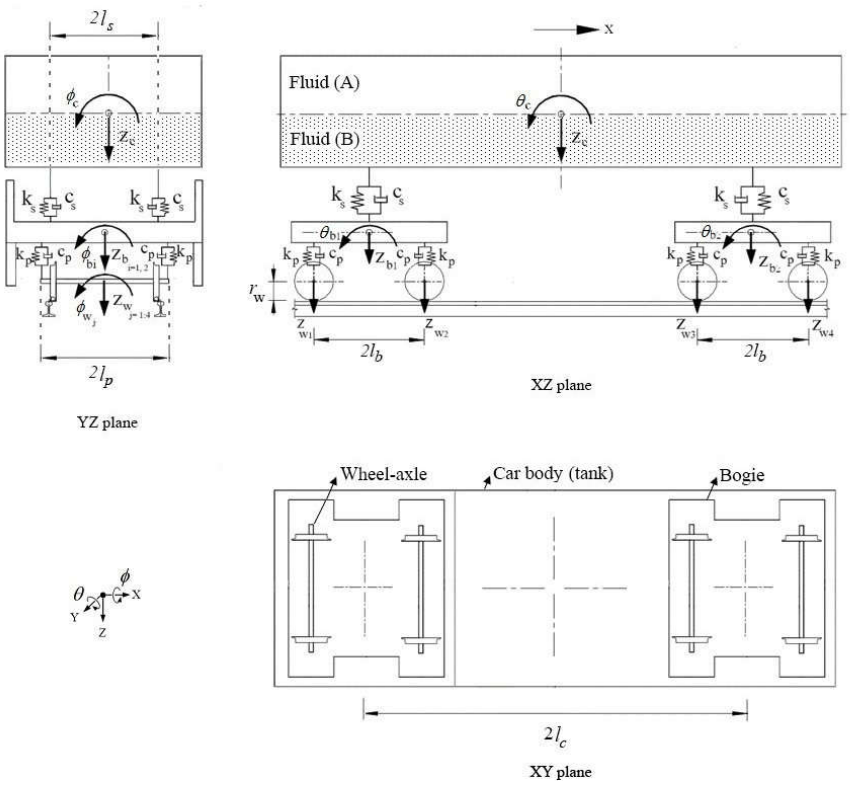

Figure 1. Wagon dynamics model

2. Wagon Dynamics Model

Here the three-dimensional model for a tank wagon is considered that includes a car body (tank), front/rear bogies and four wheel-axles. As shown in Figure 1, the dynamic system has 19 DOFs which includes vertical (z_c) , pitch (θ_c) and roll (ϕ_c) motions for car body and vertical (z_b), pitch (θ_b) and roll (ϕ_b) motions for bogies. Four wheel-axles have vertical (z_w) , Rotational (Y-axis) (θ_w) and roll (ϕ_w) degrees of freedom. The longitudinal coordinate of all components is the same.

The straight-line braking maneuvers is considered. Therefore, the lateral and yaw motion can be ignored by the wagon dynamics model. These degrees of freedom are effective on the hunting stability of the wagon moving on curved tracks.[19] The front/rear bogies are connected to the wheel-axles with the primary suspensions and linked to the car body through the secondary suspensions.

The rigidity of the rails and substrate is almost one thousand times greater than the flexibility of the wagon components [20, 21]. So, to simplify the analysis, the deformation of the rail and the substrate is neglected. All parameters of the wagon dynamics model are listed in Table 1. The differential equations of motion are obtained using the energy method.

Car body motion equations:

Vertical:

$$M_c\ddot{z}_c + 4c_s\dot{z}_c + 4k_s z_c - 2c_s\dot{z}_{b1} - 2c_s\dot{z}_{b2} - 2k_s z_{b1} - 2k_s z_{b2} = F_{fz} \quad (1)$$

Pitch:

$$J_{cy}\ddot{\theta}_c + 4c_s l_c^2\dot{\theta}_c - 2c_s l_c\dot{z}_{b1} + 2c_s l_c\dot{z}_{b2} + 4k_s l_c^2\theta_c - 2k_s l_c z_{b1} + 2k_s l_c z_{b2} = M_{fy} \quad (2)$$

Roll:

$$J_{cx}\ddot{\phi}_c + 4c_s l_s^2\dot{\phi}_c - 2c_s l_s^2\dot{\phi}_{b1} - 2c_s l_s^2\dot{\phi}_{b2} + 4k_s l_s^2\phi_c - 2k_s l_s^2\phi_{b1} - 2k_s l_s^2\phi_{b2} = M_{fx} \quad (3)$$

[DOI: 10.22068/IJRARE.7.2.19]

Bogies motion equations:

Vertical:

$$\begin{aligned} &M_{bi}\ddot{z}_{bi}+2c_s\dot{z}_{bi}-2c_s\dot{z}_c+4c_p\dot{z}_{bi}-2c_p\dot{z}_{wj}\\ &-2c_p\dot{z}_{w(j+1)}+2k_sz_{bi}-2k_sz_c+4k_pz_{bi}\\ &-2k_pz_{wj}-2k_pz_{w(j+1)}=0\\ &\begin{vmatrix} i=1\\ j=1 \end{vmatrix},\begin{vmatrix} i=2\\ j=3 \end{vmatrix} \end{aligned} \tag{4}$$

Pitch:

$$\begin{aligned} &J_{byi}\ddot{\theta}_{bi}+4c_pl_b^{\,2}\dot{\theta}_{bi}-2c_pl_b\dot{z}_{wj}+2c_pl_b\dot{z}_{w(j+1)}\\ &+4k_pl_b^{\,2}\theta_{bi}-2k_pl_bz_{wj}+2k_pl_bz_{w(j+1)}=0\\ &\begin{vmatrix} i=1\\ j=1 \end{vmatrix},\begin{vmatrix} i=2\\ j=3 \end{vmatrix} \end{aligned} \tag{5}$$

Roll:

$$\begin{aligned} &J_{bxi}\ddot{\phi}_{bi}+4c_pl_p^{\,2}\dot{\phi}_{bi}+2c_sl_s^{\,2}\dot{\phi}_{bi}-2c_pl_p^{\,2}\dot{\phi}_{wj}\\ &-2c_pl_p^{\,2}\phi_{w(j+1)}-2c_sl_s^{\,2}\dot{\phi}_c+4k_pl_p^{\,2}\phi_{bi}\\ &+2k_sl_s^{\,2}\phi_{bi}-2k_pl_p^{\,2}\phi_{wj}-2k_pl_p^{\,2}\phi_{w(j+1)}\\ &-2k_sl_s^{\,2}\phi_c=0\\ &\begin{vmatrix} i=1\\ j=1 \end{vmatrix},\begin{vmatrix} i=2\\ j=3 \end{vmatrix} \end{aligned} \tag{6}$$

Wheel-axels motion equations:

Vertical:

$$\begin{aligned} &M_w\ddot{z}_{wj}+2c_p\dot{z}_{wj}-2c_p\dot{z}_{bi}+2c_pl_b\dot{\theta}_{bi}\\ &+2k_pz_{wj}-2k_pz_{bi}+2k_pl_b\theta_{bi}+P_{WRj}=0\\ &\begin{vmatrix} i=1\\ j=1,2 \end{vmatrix},\begin{vmatrix} i=2\\ j=3,4 \end{vmatrix} \end{aligned} \tag{7}$$

Rotational (Y-axis):

$$J_{wyi}\ddot{\theta}_{wi}+2F_{WR}r_w+2T_b=0 \qquad i=1,...,4 \tag{8}$$

Roll:

$$\begin{aligned} &J_{wxj}\ddot{\phi}_{wj}+2c_pl_p^{\,2}\dot{\phi}_{wj}-2c_pl_p^{\,2}\dot{\phi}_{bi}+2k_pl_p^{\,2}\phi_{wj}\\ &-2k_pl_p^{\,2}\phi_{bi}+M_{WRj}=0\\ &\begin{vmatrix} i=1\\ j=1,2 \end{vmatrix},\begin{vmatrix} i=2\\ j=3,4 \end{vmatrix} \end{aligned} \tag{9}$$

Longitudinal motion equation:

$$\begin{aligned} &(M_c/4+M_b/2+M_w)\ddot{x}-2F_{WR}\\ &-F_{fx}/4=0 \end{aligned} \tag{10}$$

The effect of transient sloshing in In (1)-(3), and (10) is considered as forced vibration terms include longitudinal and vertical sloshing forces (F_{fx},F_{fz}), longitudinal and lateral sloshing moments (M_{fx},M_{fy}). According to (11) the braking torque is adopted in (8) as T_b which is applied to the wheel-axles [22].

$$T_b=T_{b\max}(1-e^{-t}) \tag{11}$$

Where $T_{b\max}$ is the final braking torque. According to (11), the time delay of applying the brake torque relative to the wagon system distance from the locomotive is neglected. The wheel-rail contact is considered based on nonlinear Hertzian contact and Kalker's theory. Figure 2 shows the wheel-rail contact model. According to (12)-(15) based on the nonlinear Hertzian theory, the resultant vertical contact is calculated as the forces (P_{WR}) and moments (M_{WR}) of the contact region.

In (10) F_{WR} is the longitudinal wheel-rail contact force which is calculated as a product of the creep coefficient f_{33} and longitudinal creepage ζ_x based on Kalker's theory (16). f_{33} is defined by the Kalker [23] and ζ_x is calculated from (17).

[DOI: 10.22068/IJRARE.7.2.19]

$$P_{WRlj}(t)=\begin{cases}c_H\left[z_{wj}(t)-l_p\phi_{wj}(t)\right]^{3/2}\\ 0\end{cases}\quad \begin{matrix}z_{wj}(t)-l_p\phi_{wj}(t)>0\\ z_{wj}(t)-l_p\phi_{wj}(t)\le 0\end{matrix}, \tag{12}$$

$$\nabla.V=0 \tag{18}$$

$$\frac{\partial V}{\partial t}+\nabla.(\nabla V)=-\frac{1}{\rho}\nabla p +\frac{1}{\rho}\nabla.\mu(\nabla V+(\nabla V)^T)+F_f \tag{19}$$

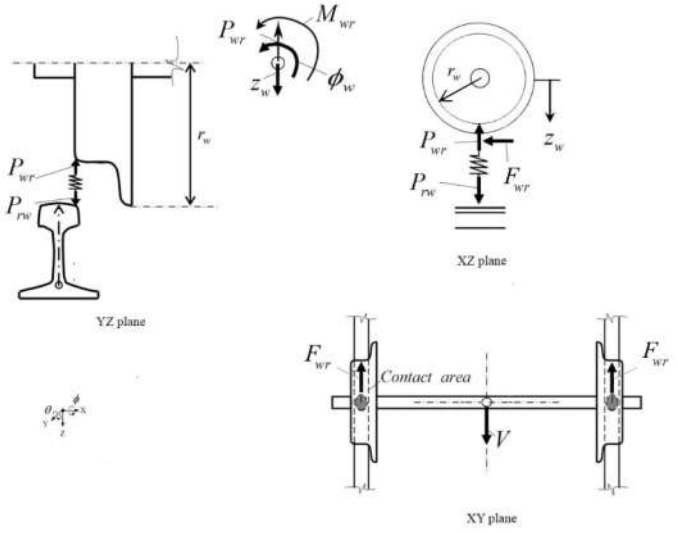

Figure 2. Wheel-rail contact model

$$P_{WRrj}(t)=\begin{cases}c_H\left[z_{wj}(t)+l_p\phi_{wj}(t)\right]^{3/2}\\ 0\end{cases}\quad \begin{matrix}z_{wj}(t)+l_p\phi_{wj}(t)>0\\ z_{wj}(t)+l_p\phi_{wj}(t)\le 0\end{matrix}, \tag{13}$$

$$P_{WRj}(t)=P_{WRrj}+P_{WRlj} \tag{14}$$

$$M_{WRj}(t)=\left[P_{WRlj}(t)-P_{WRrj}(t)\right]l_p \tag{15}$$

$$F_{WR}=-f_{33}\zeta_x \tag{16}$$

$$\zeta_x=\frac{\left|\dot{x}_w\right|-\left|r_w\dot{\theta}_w\right|}{\dot{x}_w} \tag{17}$$

3. Transient Fluid Slosh Model

The incompressible fluid flow in a partially-filled tank is determined by solving the continuity and Navier–Stokes mass conservation equations.

Where ∇ is gradient operator. v , p , ρ and μ are velocity vector, pressure, density and dynamic viscosity of fluid respectively. F_f is body force (per unit volume) applied to the fluid due to gravity and external acceleration, e.g. vehicle manoeuvers.

Table 1. Mechanical properties of wagon dynamics model

Notation	*Value*	*Unit*
M_c, M_b, M_w	8508, 1700, 1120	kg
J_{cx} , J_{cy}	13739, 129315	$kg.m^2$
J_{bx} , J_{by}	1600, 760	$kg.m^2$
J_{wx} , J_{wy}	420.1, 70.1	$kg.m^2$
k_p, k_s	7.88×10^8, 5.32×10^6	$\frac{N}{m}$
c_p, c_s	$3.5\times10^3, 7\times10^4$	$\frac{N.s}{m}$

[DOI: 10.22068/IJRARE.7.2.19]

l_b , l_p , l_c , l_s	5.8 , 0.8 , 1.25 , 0.8	m
c_H	87×10^9	$\frac{N}{m^{3/2}}$
$T_{b\max}$	2000	$N.m$
r_w	0.475	m

The external force is determined by the sum of forces including gravitational, translational and rotational inertia forces:

$$F_f = g - \frac{dU}{dt} - \frac{d\Omega}{dt}\times r - 2\Omega\times\frac{dr}{dt} - \Omega\times(\Omega\times r) \quad (20)$$

Where r , U and Ω are position vector of the fluid particle, translational velocity vector and angular velocity vector respectively. The external force vector, F_f , is used in the Navier–Stokes equations (19).

Fluid slosh in the tank is a type of two-phase flow involving liquid and gas phases. The VOF technique can track the advection of the fluid interface in moving tanks.[15, 24, 25] This method is used to model the two immiscible fluid by solving two single set of momentum equations and solving volume fraction function f coupled with velocity V .

$$\frac{\partial f}{\partial t} + \nabla.(Vf) = 0 \quad (21)$$

$$\rho = f_2\rho_2 + (1-f_2)\rho_1 \quad (22)$$

$$\mu = f_2\mu_2 + (1-f_2)\mu_1 \quad (23)$$

The volume fraction has value, either 1 or 0. Zero represents a cell filled with gas and unity value refers to a cell occupied by the liquid. Here, the first phase is air (Fluid A) and the second phase is water (Fluid B) as shown in

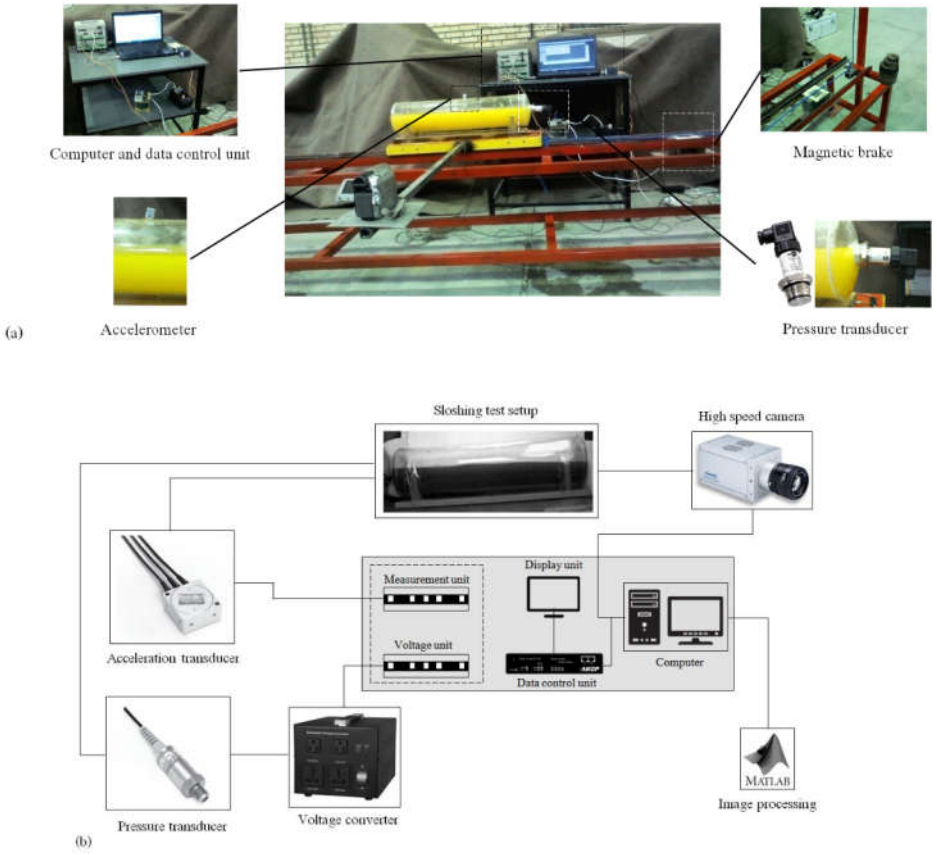

Figure 3. Sloshing test setup. a) Setup component. b) Performance process

[DOI: 10.22068/IJRARE.7.2.19]

Figure 1. The fluid flow can be assumed to be laminar since fluid slosh under typical longitudinal manoeuvres occurs at low velocity [13]. In this paper, CFD commercial software ANSYS FLUENT with VOF technique is used to solve transient fluid slosh equations.

At any time step, the sloshing force is computed by integrating the pressure over the wetted tank wall and the moment is obtained by cross-product of the position vector r_i and the force vector F_i over wetted faces cell.

$$F(t) = \sum_{Q} P_i . A_i \tag{24}$$

$$M(t) = \sum_{Q} \overline{r_i} \times F_i \tag{25}$$

Where P_i is the pressure and A_i the area vector of the i th wall cell. Q indicates the domain of wetted face of the tank and r_i is the position vector of the wall cell from the origin of the tank coordinate system.

3.1. Validation and sloshing test setup

In this section, the validation of the CFD model is performed with the experimental data. The sloshing test setup is established for a scaled model. Figure 3-a shows the configuration of the test setup. The body of the tank is of plexiglass, which has sufficient transparency to track the free surface of the fluid flow. The straight-line acceleration process is carried out on a 3-meter rail track. The test setup components include a pressure transducer, accelerometer, high-speed camera and computer with the data control unit.

According to Figure 3b, the free surface of the fluid, the fluid slosh pressure and tank acceleration are measured by the high-speed camera (image processing method), pressure transducer and accelerometer, respectively. Figure4 shows the dimensions of the real tank model and fluid domain discretization in the CFD simulation. To simplify the test, the model is scaled with a ratio of 0.048 by circular cross-section.

CFD simulation and fluid slosh test for 30% filling volume are investigated. Figure 5 shows the acceleration of the tank measured with the accelerometer. The longitudinal and vertical accelerations depend on longitudinal tank speed and rail irregularities respectively. The clearance between wheel and rail causes the acceleration along the y-axis to be significant (Figure 5-d). The free surface of the fluid is compared in Figure 6. As can be seen, wave profiles and free surface elevation in two models have a good agreement.

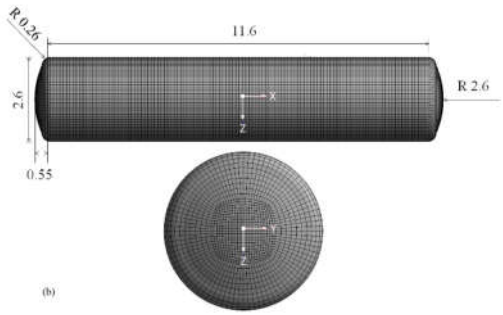

Figure 4. Fluid mesh tank geometry of real tank (dimensions in meter)

Since the suspension system is not used in experimental setup e.g. rigid foundation for the system according to Fig 5-d, the validation of the numerical results is performed only for fluid slosh (CFD) model. After being assured of CFD model settings and results in ANSYS-FLUENT, the coupled model is established.

4. Coupling of Wagon Dynamics and Fluid Slosh Models

The numerical calculations are carried out in two subsystems, including the wagon dynamics and the fluid slosh models, so that the input and output data between MATLAB and FLUENT software are exchanged using the User-Defined Function (UDF) utility. Figure 7 illustrates the computational process in the coupled model. Initially, according to the predefined calculation time step in the wagon dynamics model, the vibration parameters of the car body is computed including rotational velocities $[\dot{\theta}_c, \dot{\phi}_c]$ and translational/rotational accelerations $[\ddot{x}_c, \ddot{z}_c, \ddot{\theta}_c, \ddot{\phi}_c]$.

These outputs transmitted to the fluid slosh model in (20) by coordinate system transformation. The negative sign in (25) illustrates that the fluid flow is in the opposite direction of the tank movement. This model

[DOI: 10.22068/IJRARE.7.2.19]

calculates the fluid slosh parameters, including the longitudinal slosh force (F_{fx}), vertical slosh force (F_{fz}), longitudinal slosh moment (M_{fx}) and lateral slosh moment (M_{fy}), which at $t_{i+1} = t_i + \Delta t$ transmitted to the wagon dynamics model in (1)-(3) and (10) as the forced vibration terms by coordinate system transformation. The process is repeated until the end time.

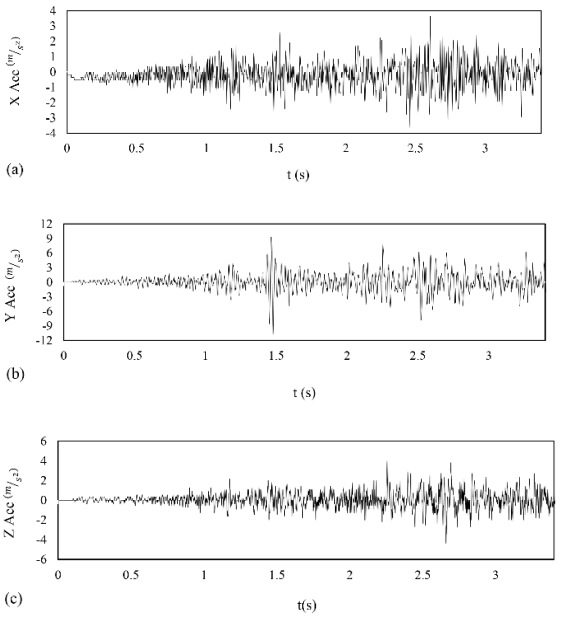

Figure 5. 3D accelerometer a) Longitudinal b) Lateral c) Vertical d) Wheel-rail contact

The center of the coordinate system coincides in the wagon dynamics and the fluid slosh models. The wagon dynamics model is solved by the fourth-order Runge-Kutta method using MATLAB. In the CFD analysis, the first-order discretization in the space and time domain is used.

5. Results and Discussion

The coupled model of the wagon dynamics and the fluid slosh models for a water-filled railway tank wagon is developed. The braking acceleration of the partially filled railway tank wagon is usually less than 0.08 g. Here, normal braking manoeuvre is applied with initial velocity $5 m/s$ by applying the braking torque to the wheel-axles according to (11).

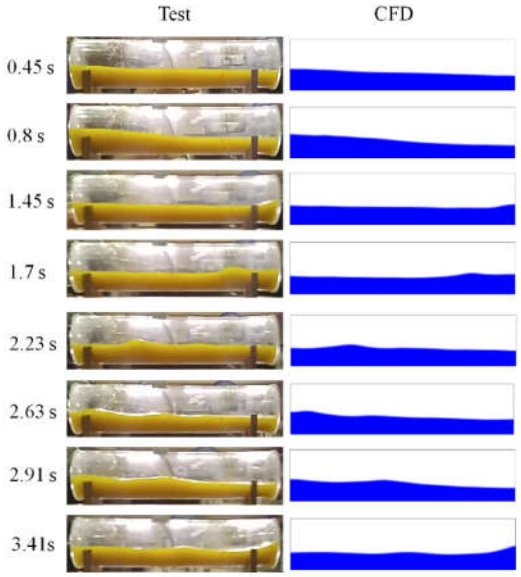

Figure 6. CFD model and experimental results

For convergence of results e.g. instability analysis, the effect of time step and the number of cells must be checked. The transient fluid slosh model is analyzed for 81900, 132352 and 211276 cells. Then the time steps 0.01s and 0.001s are investigated. According to Figure 8 good agreement for the longitudinal centre of gravity CG_x is observed. Therefore the 132352 cells and $\Delta t = 0.01s$ is sufficient for convergence analysis. The instability analysis is performed for the coupled model with more complicated conditions of data exchange between the two models (Figure 7), so for both subsystem, the effect of time step and cell size is confirmed.

5.1. Filling volume effect

[DOI: 10.22068/IJRARE.7.2.19]

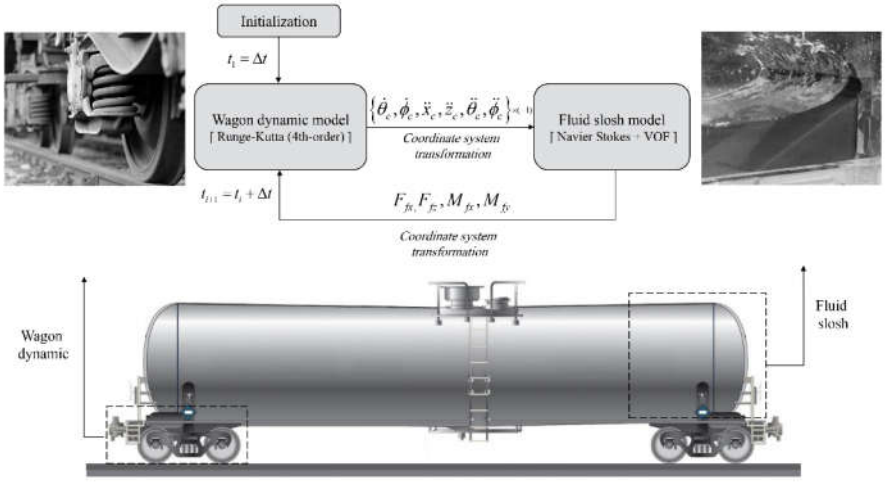

Figure 7. Computational process of coupled wagon dynamics-fluid slosh model

In this section, the filing volume effect on various parameters including center of gravity coordinate for fluid, force and moment of fluid slosh and dynamic response characteristics of tank wagon is investigated. The results are obtained until $t = 80s$ because of the large computational time in the coupled model. Fig. 9(a-b) shows the center of gravity coordinate in the longitudinal CG_x and vertical directions CG_z respectively for 30%, 50%, and 70% filling volume.

As can be seen, higher filling volume reduces the centre of gravity coordinate in both directions. Figure 9 also illustrate that changes in amplitude and frequency of the longitudinal centre of gravity coordinate are greater than the vertical direction as expected because the braking manoeuvre in the longitudinal direction will exert more excitation on the fluid domain.

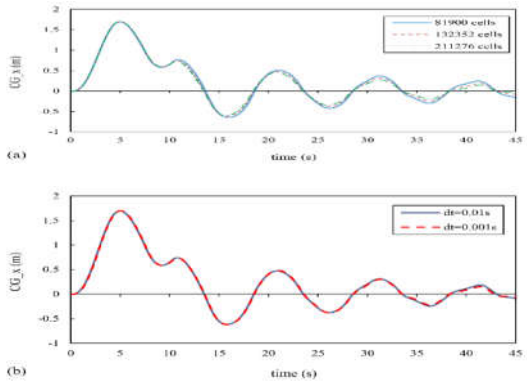

Figure 8. Convergence analysis of the number of cells (a) and time step (b)

According to Figure 10, a higher filling volume of the tank causes a higher braking time because the longitudinal slosh force is increased as shown in Figure 12a. Table 2 shows the lowest braking acceleration and the maximum stopping distance corresponds to a 70% filling volume. The stopping time of the tank wagon for 30%, 50% and 70% filling volume is 10.4 s, 14.2s and 18s respectively as indicated in Figure 9-a.

After these times, the longitudinal acceleration of the wagon system is zero, so the second term is removed from (25). It is obvious that after the stopping times specified in Figure 9-a the amplitude of longitudinal/vertical centre of gravity coordinate is decreased with the higher rate.

Table 2. Braking acceleration and stopping distance

Filling volume (%)	***Fluid Mass*** (kg)	***Maximum braking acceleration*** (m/s^2)	***Stopping distance*** (m)
30	19481	0.64	27.5
50	32416	0.49	37.4
70	45351	0.37	47

[DOI: 10.22068/IJRARE.7.2.19]

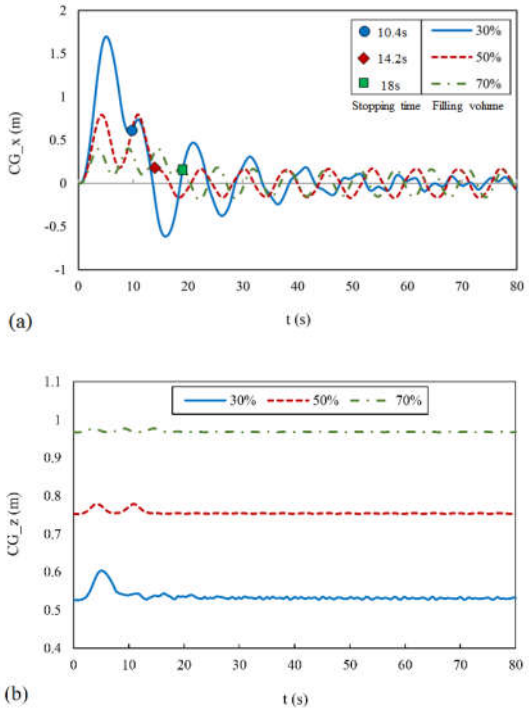

Figure 9. Center of gravity coordinate. a) Longitudinal, b) Vertical

Figure 11 shows the free surface of the fluid with 30%, 50% and 70% filling volume at different times. At $t \geq 21s$ the fluid oscillation for 50% and 70% conditions is sharply reduced, but in the 30% filling volume, the free surface of the water still fluctuates. The back-and-forth motion of fluid in the longitudinal direction continues to reach its steady state. Because of the long length of the tank (12.5m), it will take more than 80s for the fluid to reach a steady state.

The longitudinal force (F_{fx}) and lateral moment (M_{fy}) of the fluid slosh for 30%, 50%, and 70% filling volumes are shown in Figure 12. As shown in Figure 12a, higher filling volumes cause to increase the longitudinal force applied to the tank.

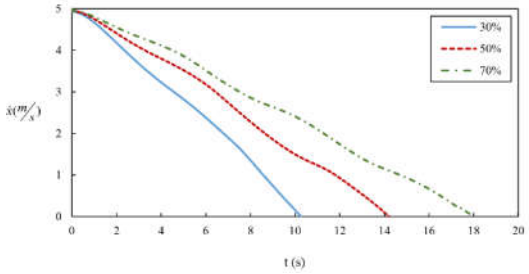

Figure 10. Longitudinal velocity of the tank wagon.

According to Figure 12b, the maximum lateral fluid slosh moment is related to 30% condition. This is because in (25), position vector, according to the longitudinal centre of gravity coordinate (Figure 9a) is much larger than the 50% and 70% filling volumes.

It is clear by increasing the filling volume the fluid behaviour is similar to a rigid cargo state, as a result, the oscillation of the force and the moment of fluid slosh decreases. Therefore according to Figure 13-a the frequency and amplitude of vertical vibrations for the car body are reduced. The minimum vertical displacement for the car body occurs at 70% filling volume. As shown in Figure 13-b the pitch angle of the car body is greater for the 30% filing volume at $t < 30s$. That's because in (2) the lateral fluid slosh moment at this time is more than other states (Figure 12-b). As can be seen, fluid slosh has a relatively small effect on the dynamic response of the car body. This can be attributed to the normal barking acceleration (less than $0.8\,{}^{m}/_{s^2}$) and the high-secondary suspension properties for heavy freight wagons.

As expected, the fluid slosh has a very slight effect on roll DOF of the car body (with order 10^{-5} rad).

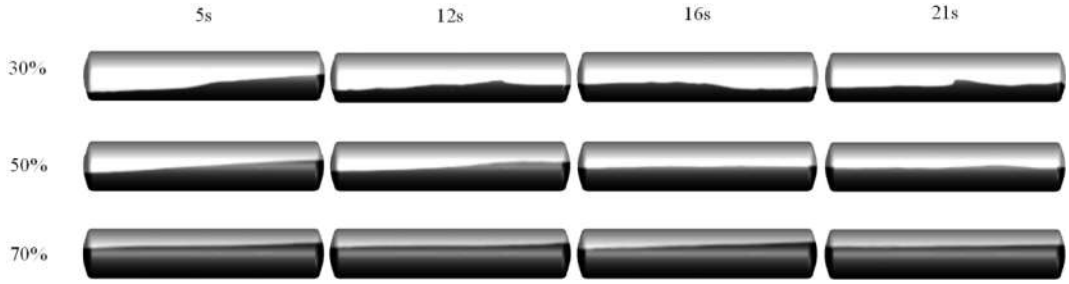

Figure 11. Free surface of fluid at 30%, 50%, 70% filling volumes

[DOI: 10.22068/IJRARE.7.2.19]

In reality, in the longitudinal fluid slosh condition, in other words, at straight line braking manoeuvre the longitudinal fluid slosh moment M_{fx} and consequently roll angle ϕ_c must be approximately zero. In this paper, as shown in Figure 13-c, its value is obtained very close to zero compared with the pitch angle θ_c. The small difference observed can be related to the rounding error of the values in the numerical computation process in solving by CFD and fourth-order Runge-Kutta methods.

In addition, the increase of the roll angle after the specified time and then the decreasing trend is associated with the stopping time of the tank wagon that indicated in Figure 9-a. Therefore, the roll degree of freedom can be ignored form wagon dynamics model for reducing the computational time.

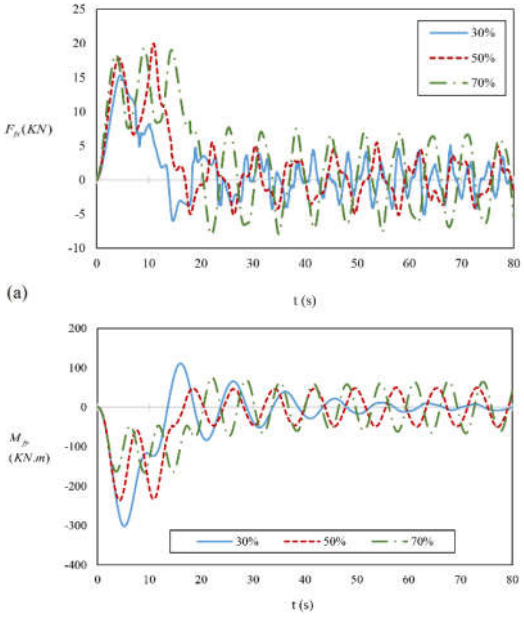

Figure 12. Transient responses of fluid slosh. a) Longitudinal force. b) Lateral moment

Dynamic characteristic for the other components such as bogies and wheel-axles are not explained due to the negligible effect of fluid slosh on their specifications. The primary and secondary suspensions can cause very small vibrations to be applied to these components.

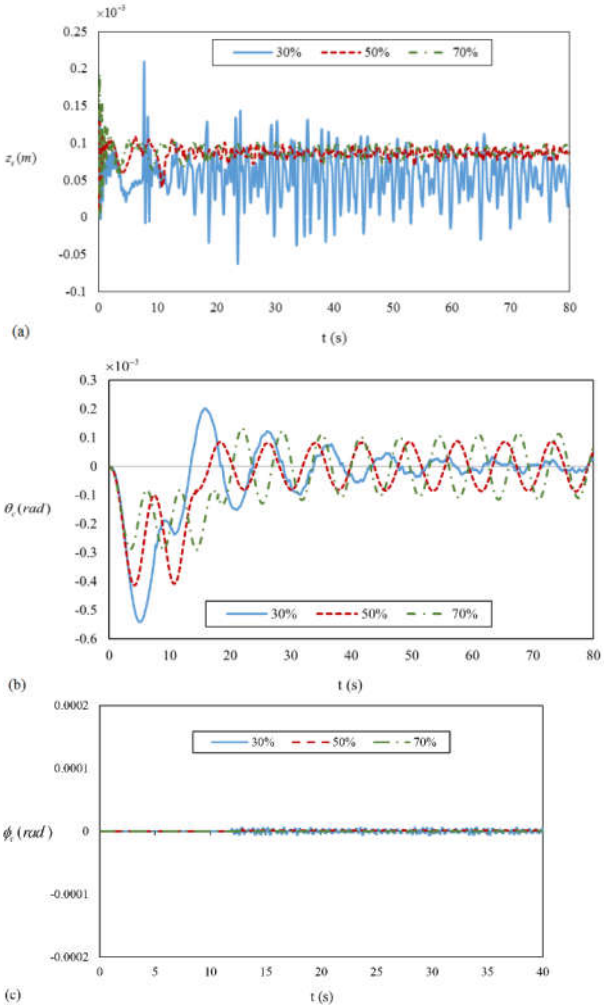

Figure 13. Dynamic response of car body. a) Vertical displacement. b) Pitch angle c) Roll angle

5.2 The effect of fluid viscosity

In this section, the effect of fluid viscosity on dynamic response characteristics of a tank wagon has been investigated in different filling volumes conditions. To study the pure effect of viscosity, the fluid is considered similar to the water properties but with a viscosity close to the viscosity of the oil. Figure14 shows the centre of gravity coordinate and longitudinal fluid slosh force in a 50% filling volume for the viscosity of water and oil.

As seen, the results are very close together and the average difference is about 1.3%. Therefore, fluid viscosity has little effect on the response of the transient fluid slosh model. In addition, the effect of fluid viscosity on the stopping distance for different filling volumes is illustrated in Figure 15.

[DOI: 10.22068/IJRARE.7.2.19]

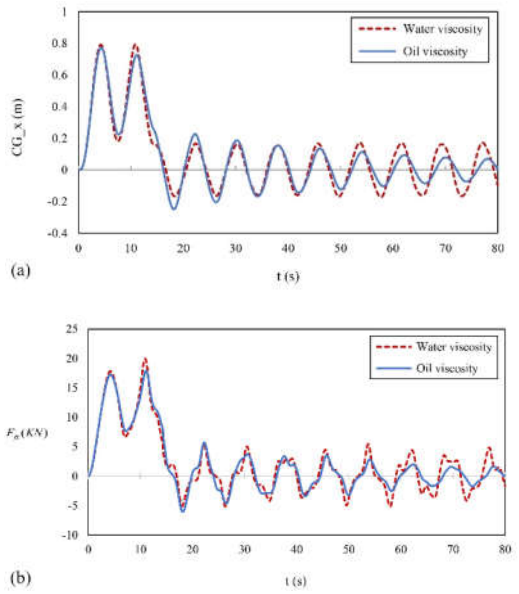

Figure 14. Fluid viscosity effect. a) Centre of gravity coordinate b) Fluid slosh force

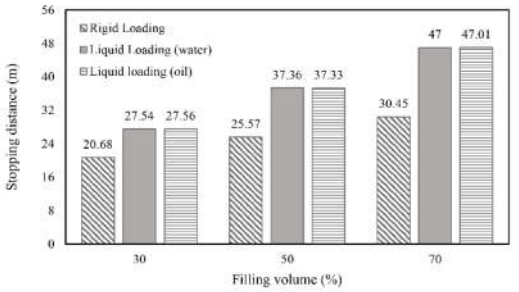

Figure 15. Stopping distance for different loading

The fluid viscosity has very little effect (order of 0.01m) on the stopping distance of the tank wagon. Also, the results are compared for rigid loading. Stopping distance is far less than liquid loading because in this situation the external excitation force is zero (1).

6. Conclusions

In this paper, an innovative method as the coupled model of wagon dynamics-transient fluid slosh is developed for the railway tanker to obtain the dynamic response under the straight line braking. For this purpose, in the coupled model, the effect of transient fluid slosh is considered in the wagon dynamics model as the term of forced vibration which is computed from the CFD method combined with the VOF technique. Wagon dynamics model with 19 DOFs including longitudinal, vertical, pitch and roll motions is solved using the fourth-order Runge-Kutta method.

The results show that the dynamic response of the tank wagon, including the longitudinal displacement and the pitch angle, are directly affected by the longitudinal fluid slosh force and the lateral fluid slosh moment, respectively. Increasing in the filling volume reduces the oscillation of the center of gravity coordinates of the fluid in both vertical and longitudinal directions. In addition, the maximum fluid slosh force and the minimum fluid slosh moment are observed in the 70% filling volume. The stopping distance and the average braking acceleration in the higher filling volume are increased and is decreased respectively. The parametric study of the fluid viscosity shows that the viscosity of the fluid has a small effect on the longitudinal fluid slosh force and the stopping distance of the tank wagon.

List of Symbols

A_i	:	*Area vector of the i th wall cell*
CG_x	:	*Fluid's centre of gravity coordinate (longitudinal)*
CG_z	:	*Fluid's centre of gravity coordinate (vertical)*
c_p	:	*Primary suspension damping*
c_s	:	*Secondary suspension damping*
c_H	:	*Hertz spring stiffness*
f	:	*Volume fraction of the liquid phase for a cell*
f_{33}	:	*Creep coefficient*

[DOI: 10.22068/IJRARE.7.2.19]

F_f	:	External force for fluid model	l_c	:	Semi-longitudinal distance between bogies
F_i		Force vector of i th wall cell			
F_{fx}	:	Longitudinal fluid slosh force	l_p	:	Semi-lateral distance between primary suspensions
F_{fz}	:	Vertical fluid slosh force			
F_{WR}	:	Wheel-rail longitudinal contact force	l_s	:	Semi-lateral distance between secondary suspensions
g	:	Gravity acceleration	M_b	:	Mass of bogie
J_{bx}	:	X-axis Inertia moments for bogie	M_c	:	Mass of car body
J_{by}	:	Y-axis Inertia moments for bogie	M_{fx}	:	X-axis Fluid slosh moment
J_{cx}	:	X-axis Inertia moments for car body	M_{fy}	:	Y-axis Fluid slosh moment
J_{cy}	:	Y-axis Inertia moments for car body	M_w	:	Mass of wheel-axle
J_{wx}	:	X-axis Inertia moments for wheel-axle	M_{WR}	:	Wheel-rail contact moment
J_{wy}	:	Y-axis Inertia moments for wheel-axle	p	:	Pressure
k_p	:	Primary suspension stiffness	P_i	:	Pressure of the i th wall cell
k_s	:	Secondary suspension stiffness	P_{WR}	:	Resultant wheel-rail hertz contact force
l_b	:	Semi-longitudinal distance between wheel-axle in bogie	P_{WRr}	:	Wheel-rail vertical contact force (right wheel)
			P_{WRl}	:	Wheel-rail vertical contact force (left wheel)
			Q	:	Wetted face on tank wall
			U	:	Translational velocity vector
			r	:	Position vector of a fluid particle

[DOI: 10.22068/IJRARE.7.2.19]

$\bar{r}_i$	:	*Position vector of wall cell from tank coordinate*
r_w	:	*Wheel radius*
T_b	:	*Braking torque*
$T_{b\max}$	:	*Final braking torque*
$\dot{x}_c$	:	*Longitudinal velocity of car body*
$\dot{x}_w$	:	*Longitudinal velocity of wheel-axle*
$\dot{z}_c$	:	*Vertical velocity of car body*
ζ_x	:	*Longitudinal creepage*
∇	:	*Gradient operator*
Δt	:	*Time step*
ρ	:	*Mass density of fluid*
μ	:	*Viscosity*
Ω	:	*Angular velocity vector*
$\dot{\theta}_c$	:	*Pitch velocity of car body*
$\dot{\phi}_c$	:	*Roll velocity of car body*
$\ddot{\theta}_c$	:	*Pitch acceleration of car body*
$\ddot{\phi}_c$	:	*Roll acceleration of car body*

References

[1]. VASIĆ, G., et al. Development of the Future Rail Freight System to Reduce the Occurrences and Impact of Derailment. in Scientific expert conference on railways RAILCON12. 2014.

[2]. Abramson, H.N., The dynamic behavior of liquids in moving containers, with applications to space vehicle technology. 1966.

[3]. Rakheja, S., S. Sankar, and R. Ranganathan, Roll plane analysis of articulated tank vehicles during steady turning. Vehicle System Dynamics, 1988. 17(1-2): p. 81-104.

[4]. Kang, X., S. Rakheja, and I. Stiharu, Cargo load shift and its influence on tank vehicle dynamics under braking and turning. International Journal of Heavy Vehicle Systems, 2002. 9(3): p. 173-203.

[5]. Cheli, F., et al., Simulation of sloshing in tank trucks. International Journal of Heavy Vehicle Systems, 2013. 20(1): p. 1-18.

[6]. Azadi, S., A. Jafari, and M. Samadian, Effect of parameters on roll dynamic response of an articulated vehicle carrying liquids. Journal of Mechanical Science and Technology, 2014. 28(3): p. 837-848.

[7]. Kolaei, A., S. Rakheja, and M.J. Richard, Range of applicability of the linear fluid slosh theory for predicting transient lateral slosh and roll stability of tank vehicles. Journal of Sound and Vibration, 2014. 333(1): p. 263-282.

[8]. Modaressi-Tehrani, K., S. Rakheja, and I. Stiharu, Three-dimensional analysis of transient slosh within a partly-filled tank equipped with baffles. Vehicle System Dynamics, 2007. 45(6): p. 525-548.

[9]. D'ALESSANDRO, V., Modeling of tank vehicle dynamics by fluid sloshing coupled simulation. 2012, Italy.

[10]. Salem, M., et al., Lateral sloshing in partially filled elliptical tanker trucks using a trammel pendulum. International Journal of Heavy Vehicle Systems, 2009. 16(1-2): p. 207-224.

[11]. Younesian, D., M. Abedi, and I. Hazrati Ashtiani, Dynamic analysis of a partially filled tanker train travelling on a curved track. International Journal of Heavy Vehicle Systems, 2010. 17(3-4): p. 331-358.

[12]. Kolaei, A., S. Rakheja, and M.J. Richard, Coupled multimodal fluid-vehicle model for analysis of anti-slosh effectiveness of longitudinal baffles in a partially-filled tank vehicle. Journal of Fluids and Structures, 2017. 70: p. 519-536.

[DOI: 10.22068/IJRARE.7.2.19]

[13]. Yan, G. and S. Rakheja, Straight-line braking dynamic analysis of a partly filled baffled and unbaffled tank truck. Proceedings of the Institution of Mechanical Engineers, Part D: Journal of Automobile Engineering, 2009. 223(1): p. 11-26.

[14]. Rahmati, A. and M. Sharavi, Volume-Filling Effects on Sloshing Frequency in Simplified and Explicit Dynamic Finite Element Models of Tank Wagons During Braking and Turning. International Journal of Railway Research, 2016. 3(1): p. 29-36.

[15]. Rumold, W., Modeling and simulation of vehicles carrying liquid cargo. Multibody system dynamics, 2001. 5(4): p. 351-374.

[16]. Thomassy, F., et al., Coupled Simulation of Vehicle Dynamics and Tank Slosh. 2003, SOUTHWEST RESEARCH INST SAN ANTONIO TX TARDEC FUELS AND LUBRICANTS RESEARCH FACILITY.

[17]. Azadi, S., A. Jafari, and M. Samadian, Effect of tank shape on roll dynamic response of an articulated vehicle carrying liquids. International Journal of Heavy Vehicle Systems, 2014. 21(3): p. 221-240.

[18]. Rahmati-Alaei, A., M. Sharavi, and M.J.P.o.t.I.o.M.E. Samadian Zakaria, Part K: Journal of Multi-body Dynamics, Development of a coupled numerical model for the interaction between transient fluid slosh and tank wagon vibration. 2018: p. 1464419318809616.

[19]. Cheng, Y.-C., S.-Y. Lee, and H.-H. Chen, Modeling and nonlinear hunting stability analysis of high-speed railway vehicle moving on curved tracks. Journal of Sound and Vibration, 2009. 324(1-2): p. 139-160.

[20]. Ishida, M., S. Miura, and A. Kono, The influence of track stiffness on track dynamic behaviour. Railway Technical Research Institute, Quarterly Reports, 1997. 38(3).

[21]. Durali, M. and M.M. Jalili. The Effect of Wheel-Rail Interactions on Wagon Dynamics in Braking. in ASME 2005 International Design Engineering Technical Conferences and Computers and Information in Engineering Conference. 2005. American Society of Mechanical Engineers.

[22]. Durali, M. and B. Shadmehri, Nonlinear analysis of train derailment in severe braking. Journal of dynamic systems, measurement, and control, 2003. 125(1): p. 48-53.

[23]. Kalker, J., Review of wheel-rail rolling contact theories. The General Problem of Rolling Contact, 1980. 40: p. 77-91.

[24]. Celebi, M.S. and H. Akyildiz, Nonlinear modeling of liquid sloshing in a moving rectangular tank. Ocean Engineering, 2002. 29(12): p. 1527-1553.

[25]. Elahi, R., M. Passandideh-Fard, and A. Javanshir, Simulation of liquid sloshing in 2D containers using the volume of fluid method. Ocean Engineering, 2015. 96: p. 226-244.

[DOI: 10.22068/IJRARE.7.2.19]